Supporting Information for

Iron (Fe) speciation in size-fractionated aerosol particles in the Pacific Ocean: The role of organic complexation of Fe with humic-like substances in controlling Fe solubility

Kohei Sakata[1,], Minako Kurisu[2], Yasuo Takeichi[3], Aya Sakaguhci[4], Hiroshi Tanimoto[1], Yusuke Tamenori[5], Atsushi Matsuki[6], Yoshio Takahash[7]*

[1]Center for Global Environmental Research, National Institute for Environmental Studies, 16-2 Onogawa, Tsukuba, Ibaraki 305-8506, Japan.

[2]Research Institute for Global Change, Japan Agency for Marine-Earth Science and Technology (JAMSTEC), 2-15, Natsushima-cho, Yokosuka, Kanagawa, 237-0061, Japan.

[3]Insituete of Materials Structure Science, High-Energy Accelerator Research Organization, Tsukuba, Ibaraki, 305-0801, Japan.

[4]Faculty of Pure and Applied Science, University of Tsukuba, 1-1-1 Tennodai, Tsukuba, Ibaraki 305-8577, Japan.

[5]Japan Synchrotron Radiation Research Institute/SPring-8, 1-1-1 Kouto, Sayo, Hyogo 679-5198, Japan.

[6]Institute of Nature and Environmental Technology, Kanazawa University, Kakuma, Kanazawa, Ishikawa 920-1192, Japan.

[7]Graduate School of Science, The University of Tokyo, 7-3-1, Hongo, Bunkyo-ku, Tokyo 113-0033, Japan.

S1. Supplemental Methods

S1.1. Estimation of available proton for mineral dust

Available proton for mineral dust ($[H^+]_{mineral}$) was estimated using the following procedures to evaluate an acidification degree of mineral dust in aerosol particles. First, NO_3^- and nss-SO_4^{2-} concentrations other than with ammonium salts were estimated using the following equation on the assumption that $[NH_4^+]_{neq}$ was present as NH_4NO_3 and $(NH_4)_2SO_4$:

$$[NO_3^- \text{ and nss-}SO_4^{2-}]_{non\text{-}NH4} = [NO_3^-] + 2\times[\text{nss-}SO_4^{2-}] - [NH_4^+] \quad \text{(Eq. 1)}$$

where $[NO_3^- \text{ and nss-}SO_4^{2-}]_{non\text{-}NH4}$ is $[NO_3^-]$ and $[\text{nss-}SO_4^{2-}]$ combined with other than NH_4^+ (e.g., Na^+ and Ca^{2+}). Then, NO_3^- and nss-SO_4^{2-} associated with Na^+ in sea spray aerosol were subtracted from $[NO_3^- \text{ and nss-}SO_4^{2-}]_{non\text{-}NH4}$. Gaseous HCl is released from sea spray aerosol by the following chemical reactions (R1 and R2):

$$NaCl\ (aq) + HNO_3\ (g) \rightarrow NaNO_3\ (aq) + HCl\ (g) \quad \text{(R1)}$$

$$2NaCl\ (aq) + H_2SO_4\ (aq) \rightarrow Na_2SO_4\ (aq) + 2HCl\ (g) \quad \text{(R2)}$$

As shown in R1 and R2, a concentration of HCl released from sea spray aerosol ($[Cl^-$ loss$]$) was released into the atmosphere. Therefore, $[NO_3^-]_{neq}$ and $[\text{nss-}SO_4^{2-}]_{neq}$ combined with Na^+ were estimated using the following equation:

$$[Cl^- \text{ loss}] = [NaNO_3] + [Na_2SO_4] = [Cl^-]_{aerosol} - ([Cl^-]_{seawater}/[Na^+]_{seawater}) \times [Na^+]_{aerosol} \quad \text{(Eq. 2)}$$

Assuming that NO_3^- and nss-SO_4^{2-} other than ammonium and Na salts were derived from heterogeneous reactions of HNO_3 and H_2SO_4 with mineral dust (e.g., $CaCO_3$), we evaluated available acids for mineral dust ($[H^+]_{mineral}$) by using the following equation:

$$[H^+]_{mineral} = [NO_3^- \text{ and nss-}SO_4^{2-}]_{mineral} = [NO_3^- \text{ and nss-}SO_4^{2-}]_{non\text{-}NH4} - [Cl^- \text{ loss}] \quad \text{(Eq. 3)}$$

When $[H^+]_{mineral}$ is negative, mineral dust in the aerosol sample is not well acidified. By contrast, positive $[H^+]_{mineral}$ means that mineral dust is acidified by secondary processes in the atmosphere.

Supplemental Figures

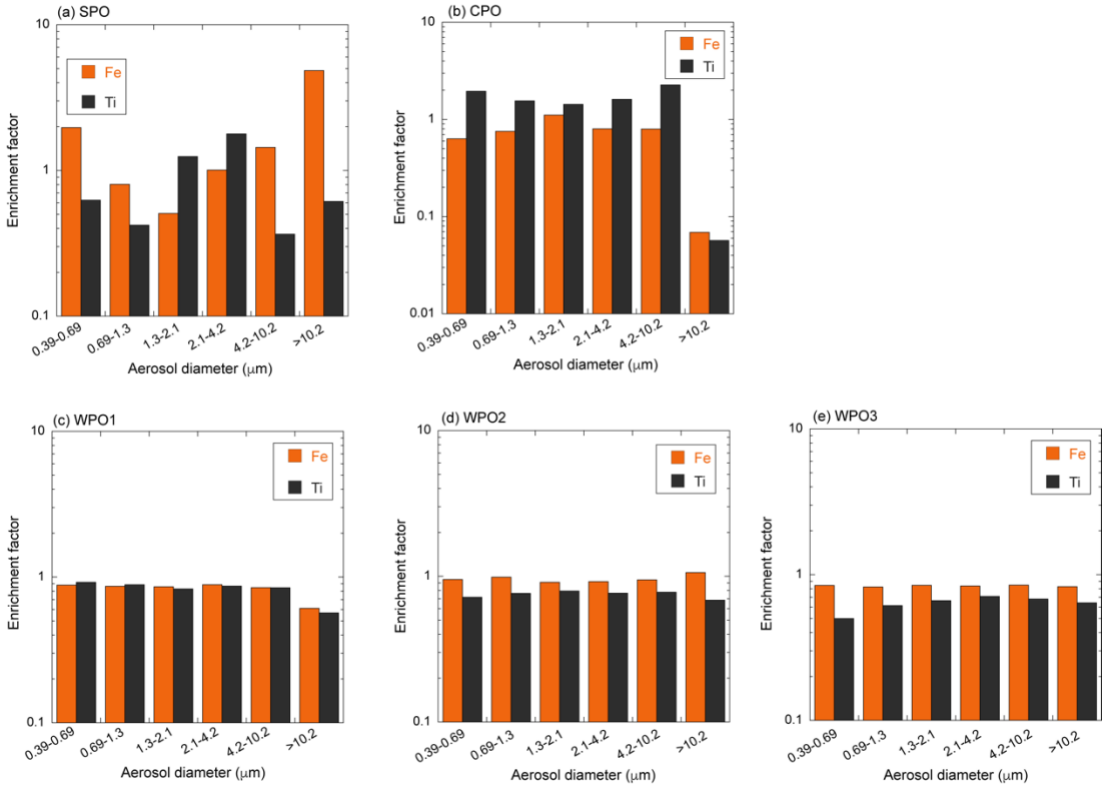

Fig. S1 Enrichment factors of Fe and Ti in size-fractionated marine aerosol particles collected in (a) SPO, (b) CPO, (c) WPO1, (d) WPO2, and (e) WPO3. Iron in these samples was derived from mineral dust because the enrichment factors of Fe were almost 1 regardless of aerosol diameter.

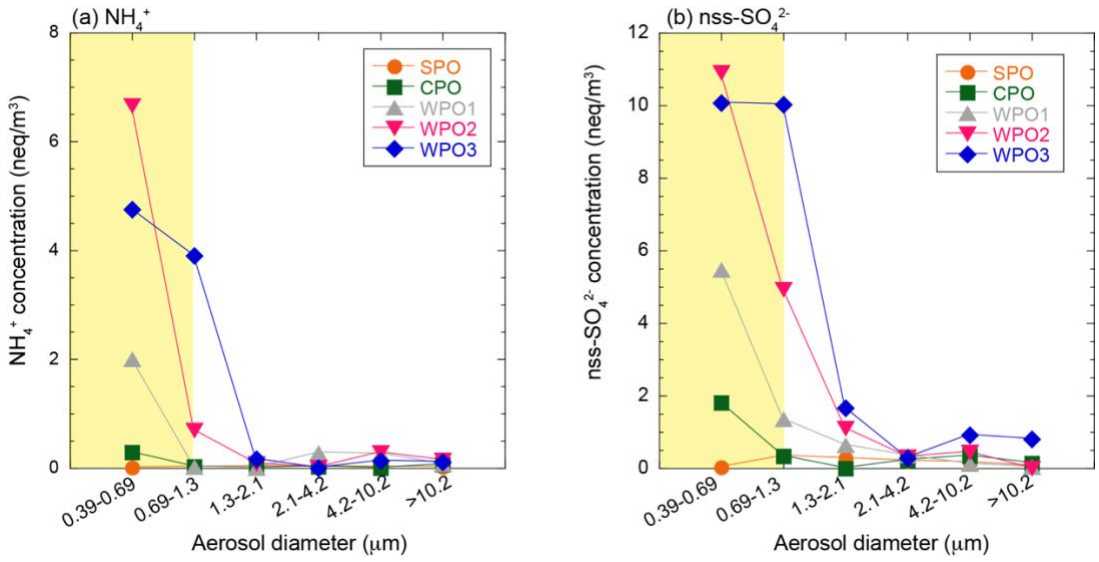

Fig. S2 Size-distributions of (a) NH_4^+ and (b) nss-SO_4^{2-} concentrations.

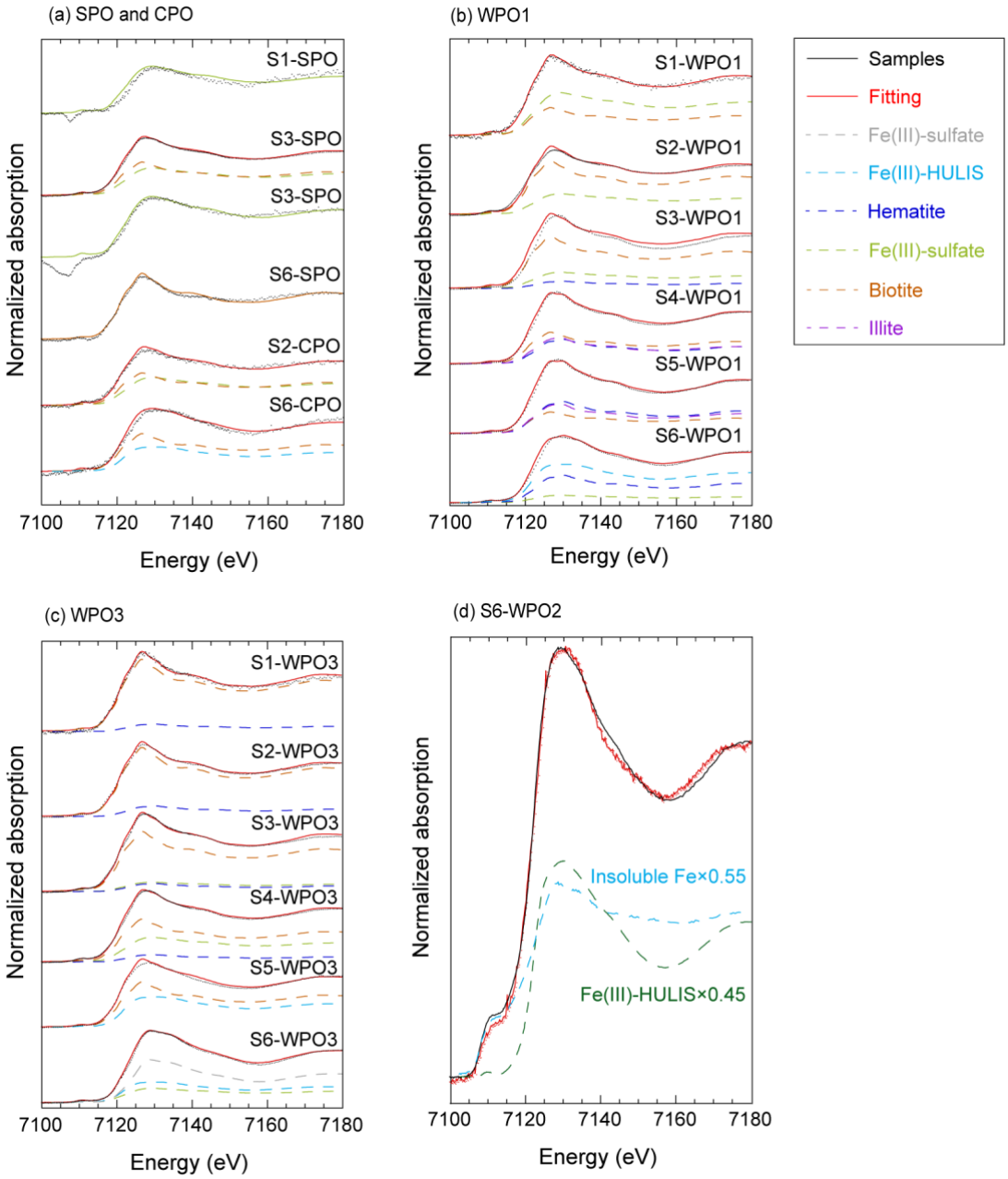

Fig. S3 Fe K-edge XANES spectra of size-fractionated aerosols in (a) CPO and SPO, (b) WPO1, (c) WPO3. XANES spectra and LCF results are represented by black and red lines, respectively. Other colors represent the components of each XANES spectrum. LCF results of stages-1, 3, and 6 in SPO are represented in light green or brown colors, as these spectra can be fitted by only one component. (d) The result of linear combination fitting of S6-WPO2 samples. The Fe K-edge XANES spectra of total Fe in S6-WPO2 was well fitted by Fe(III)-HULIS and insoluble Fe. The Fe K-edge XANES spectra of insoluble Fe was obtained from the residue of water-extraction experiment. The LCF result showed that Fe(III)-HULIS was preferentially removed from aerosol samples by water-extraction due to their high water solubility.

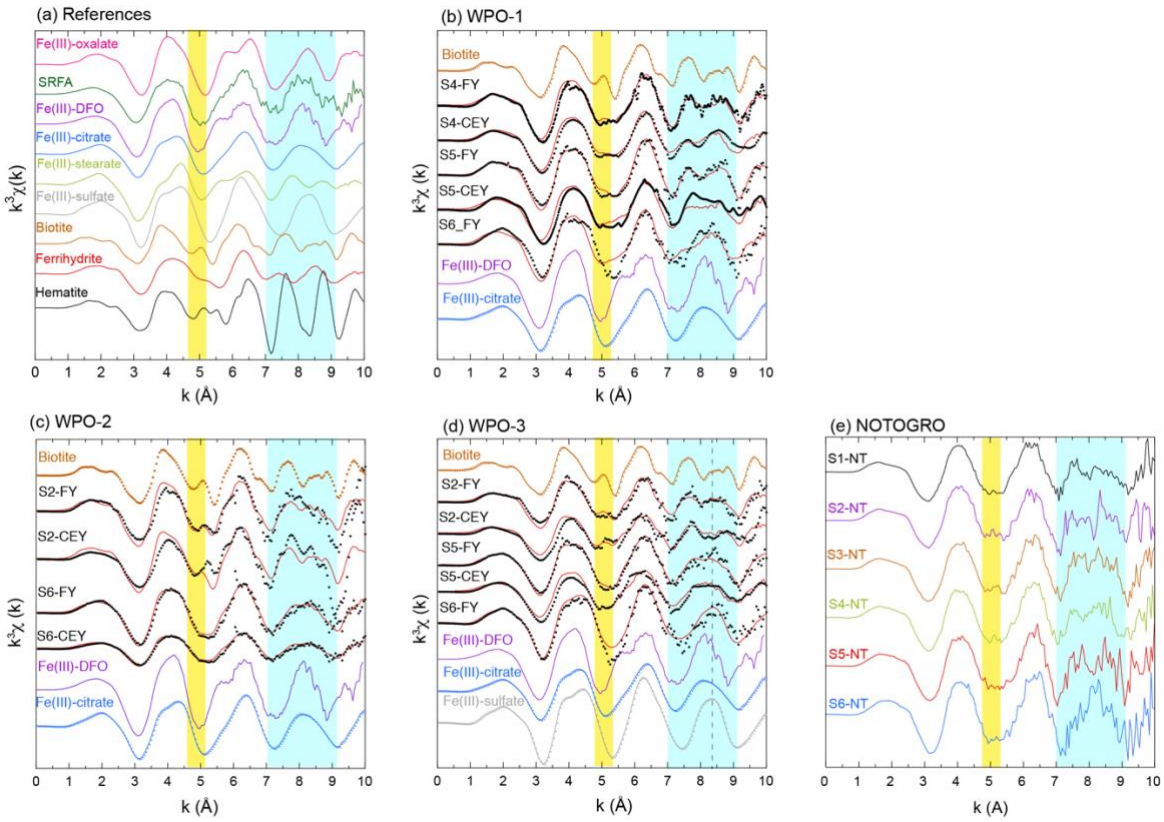

Fig. S4 Iron K-edge EXAFS spectra of the (a) reference materials, (b) WPO1, (c) WPO2, (d) WPO3, and (e) NOTOGRO. FY and CEY in panels (b-d) implied fluorescence yield (FY: bulk sensitive speciation) and conversion electron yield (CEY: surface sensitive speciation), respectively. Yellow shaded region: small peak associated with biotite could be found in EXAFS spectra of coarse aerosol particles, whereas EXAFS spectra of fine aerosol particles did not have the small peak. Light blue region: EXAFS spectra of $PM_{1.3\text{-}10.2}$ clearly reflected two peaks of biotite, whereas those of $PM_{1.3}$ have a single peak in the same region. The features of EXAFS spectra of $PM_{1.3}$ in both yellow and light blue regions were similar to those of Fe(III)-HULIS. Dashed line in panel (d) shows peak position of Fe(III)-sulfate. The peak position of S6-FY in WPO3 were similar to Fe(III)-sulfate rather than Fe(III)-HULIS.

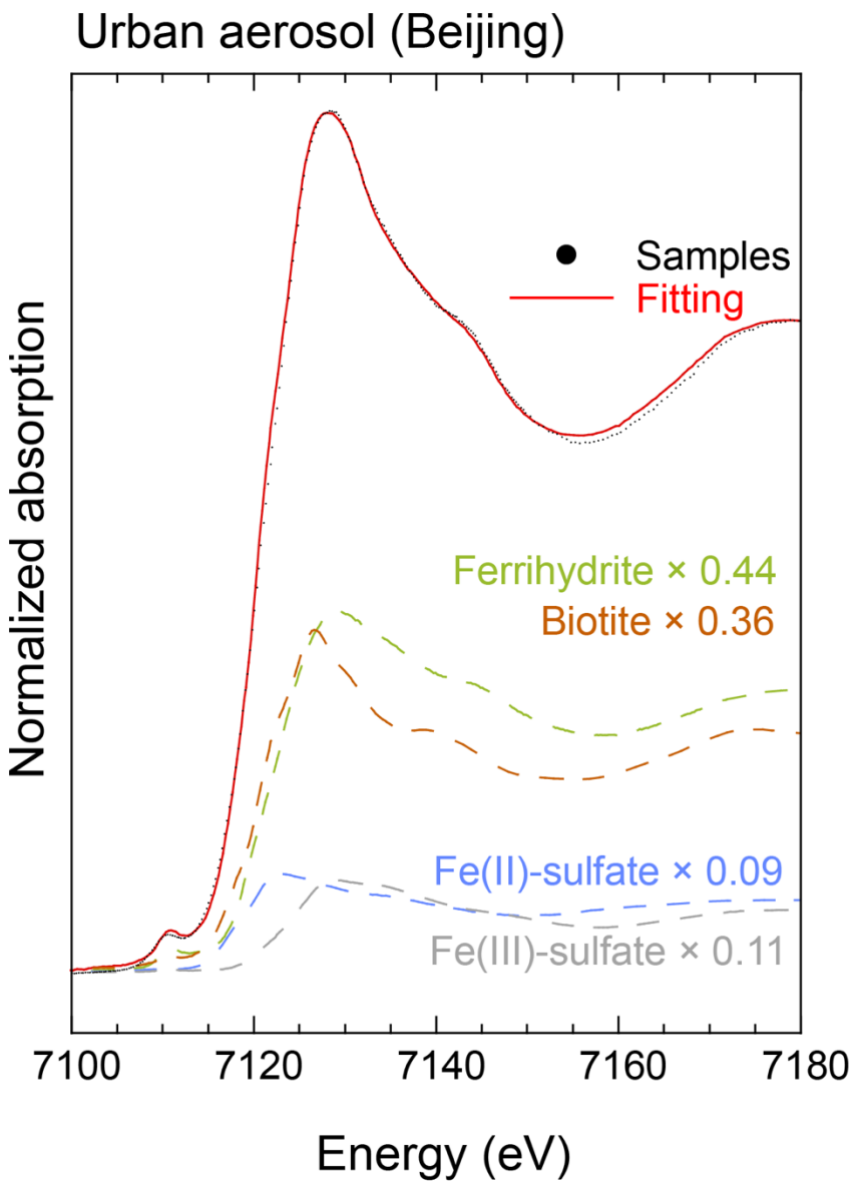

Fig. S5 Iron K-edge XANES spectra of Beijing dust and its fitting components.

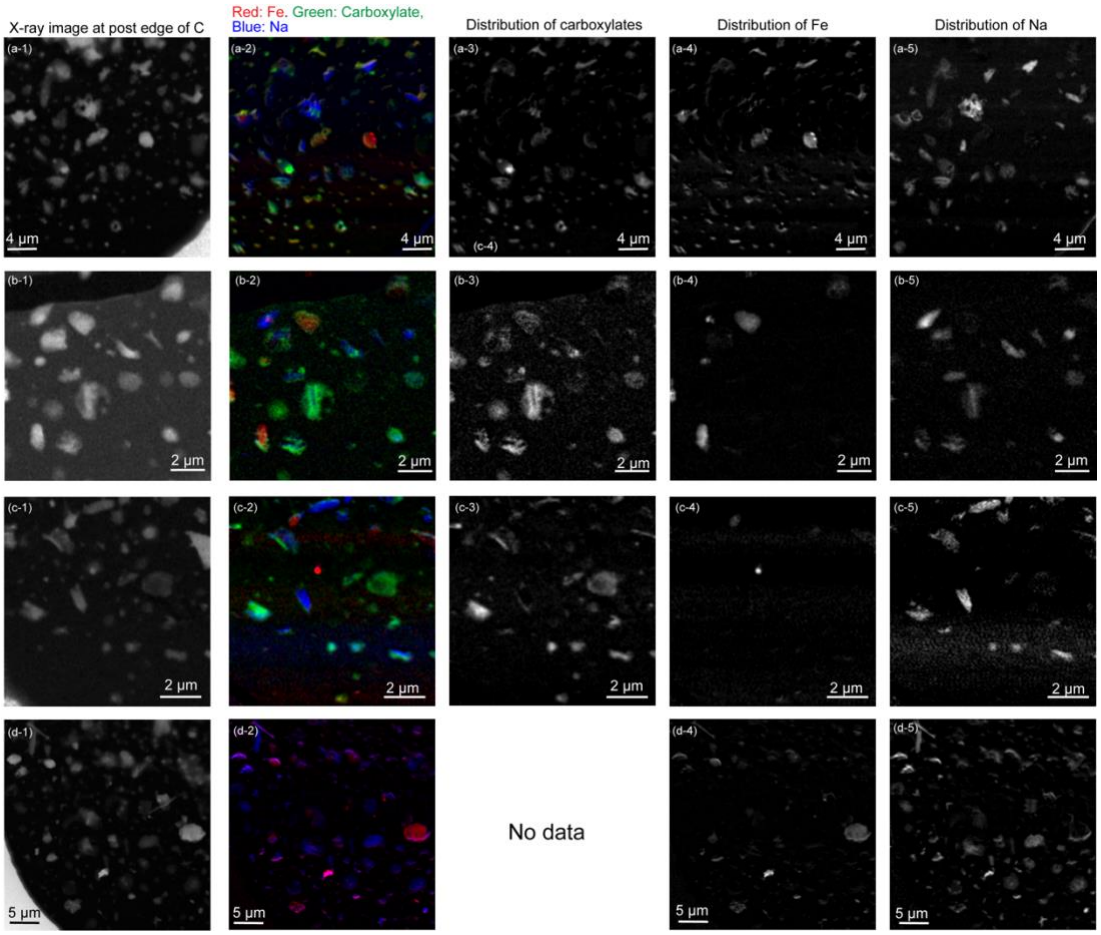

Fig. S6 (a-1 to d-1) X-ray image of S6-WPO2, (a-2 to d-2) RGB composites of Fe (red), carboxylates (green) and Na (blue). Distributions of carboxylates, Fe and, Na in the black-white scale are shown in (a-3 to b-3), (a-4 to b-4), and (a-5 to b-5), respectively.

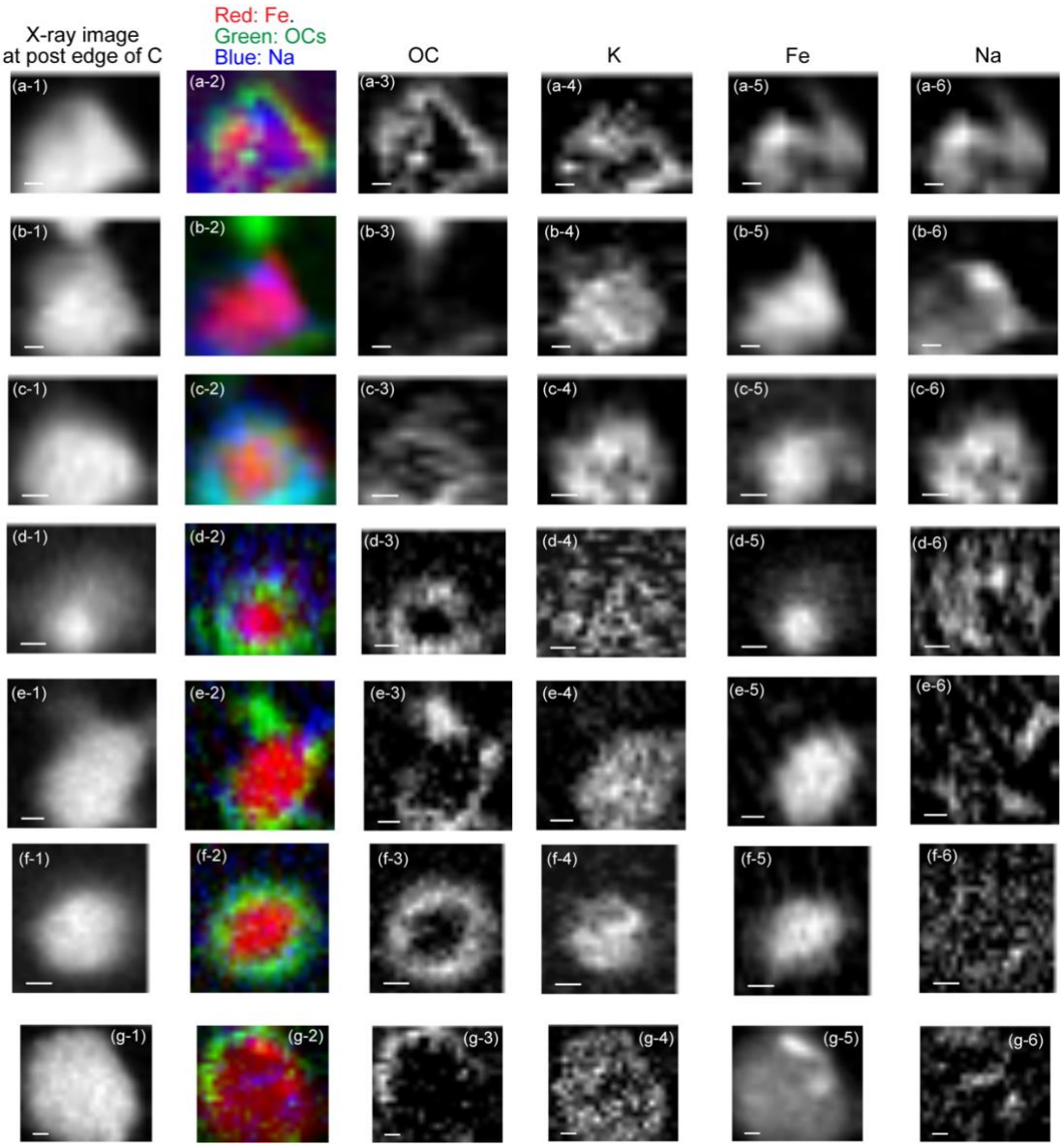

Fig. S7 (a-1 to g-1) X-ray image of phyllosilicate particles in S6-WPO2, (a-2 to g-2) RGB composite of Fe (red), carboxylates (green) and Na (blue), (a-3 to g-3) distribution of OCs, (a-4 to g-4) distribution of potassium (K), (a-5 to g-5) distribution of Fe, and (a-6 to g-6) distribution of Na.

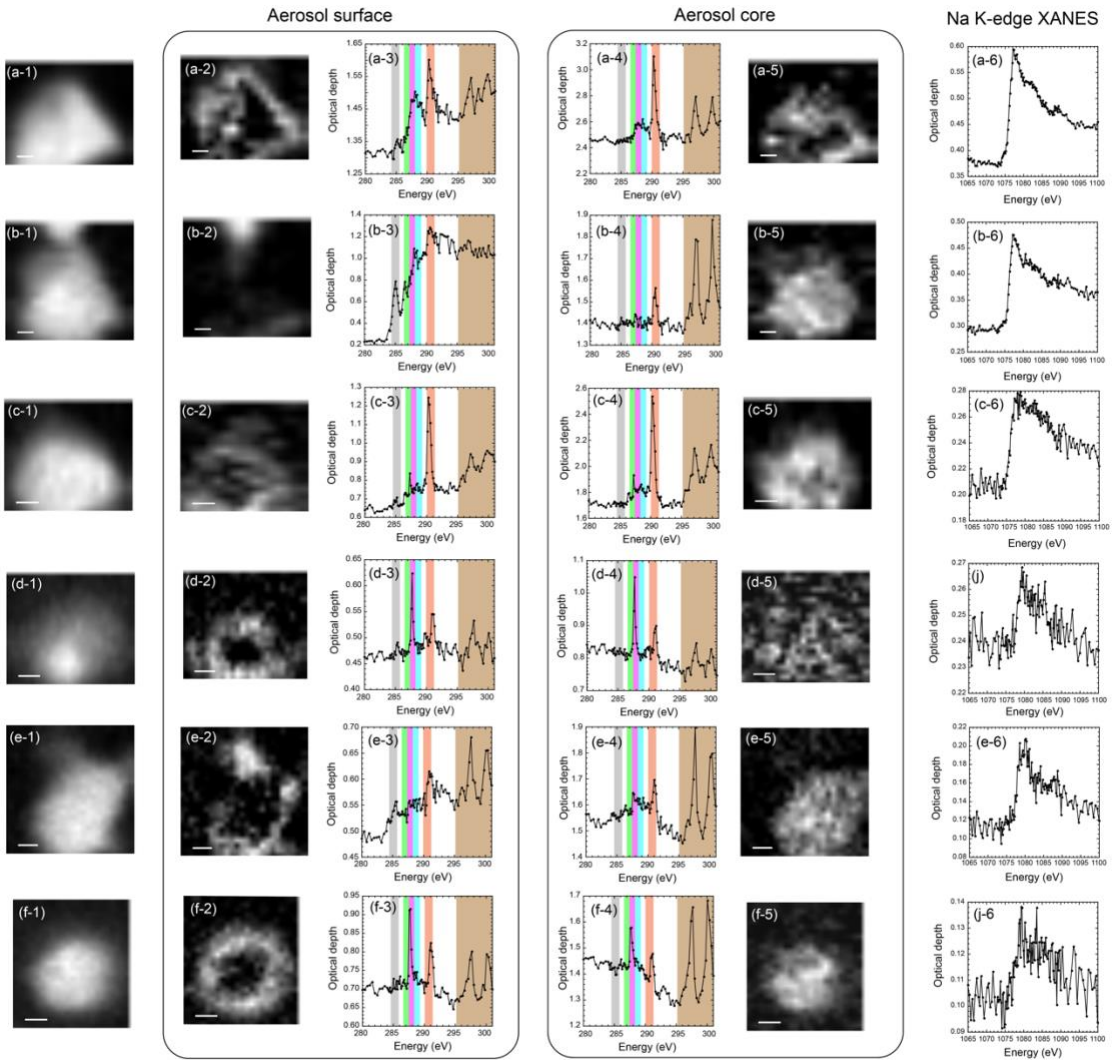

Fig. S8 (a-1 to f-1) X-ray image of phyllosilicate particles of S6-WPO2, (a-2 to f-2) distribution of OCs, (a-3 to e-3 and a-4 to f-4) Carbon K-edge and potassium L-edge XANES spectra on the aerosol surface and in the aerosol core, respectively. Gray, light green, pink, light blue, orange, and brown regions show peak position of aromatic C, ketonic C, aliphatic C, carboxylates, carbonate, and potassium, respectively. (a-5 to e-5) distribution of potassium (K). (d) Na K-edge XANES spectra on the aerosol surface.

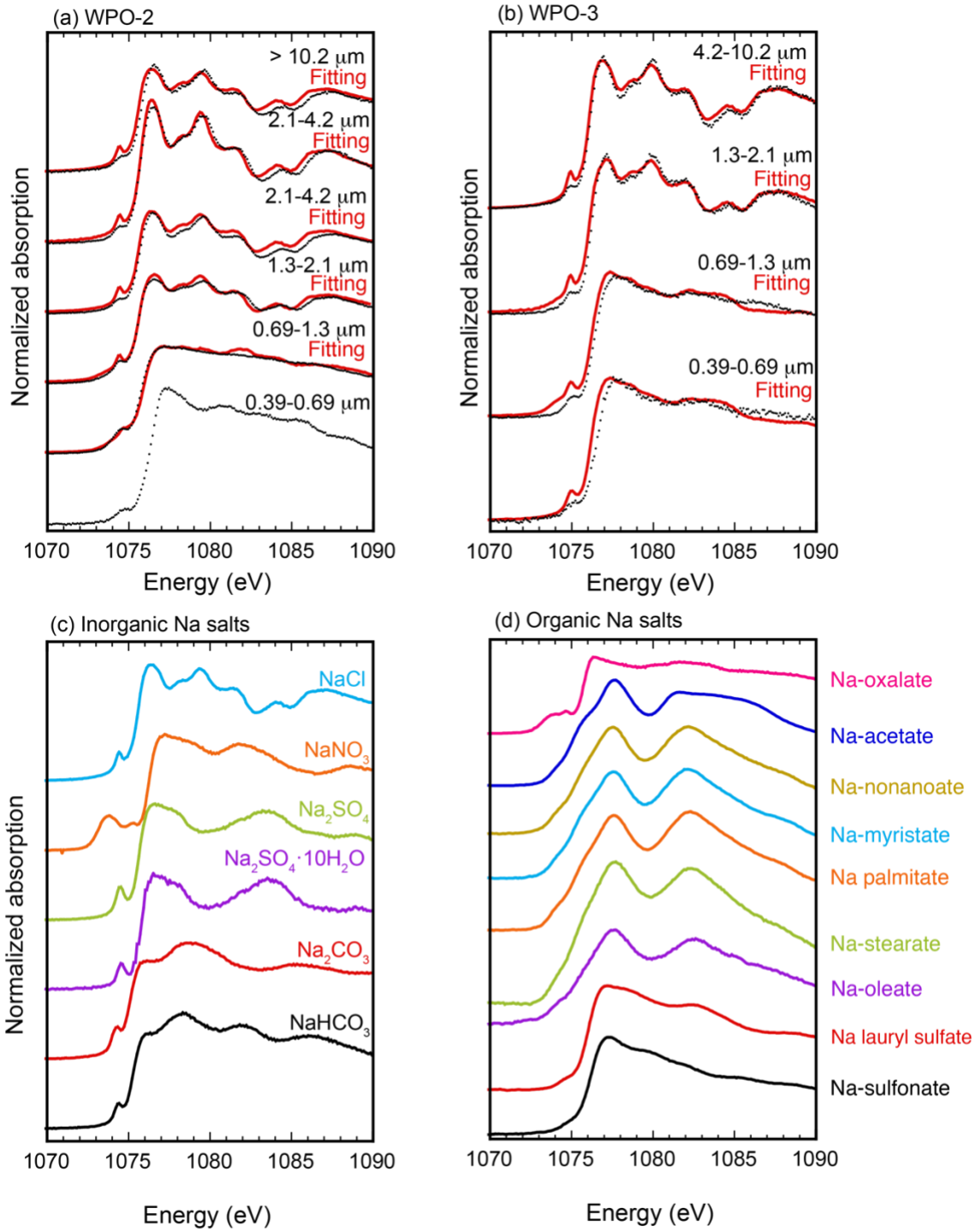

Fig. S9 Na K-edge XANES spectra in size-fractionated aerosol samples collected in (a)WPO2 and (b) WPO3. The XANES spectra of reference materials of inorganic and organic Na salts are shown in panels (c) and (d), respectively.

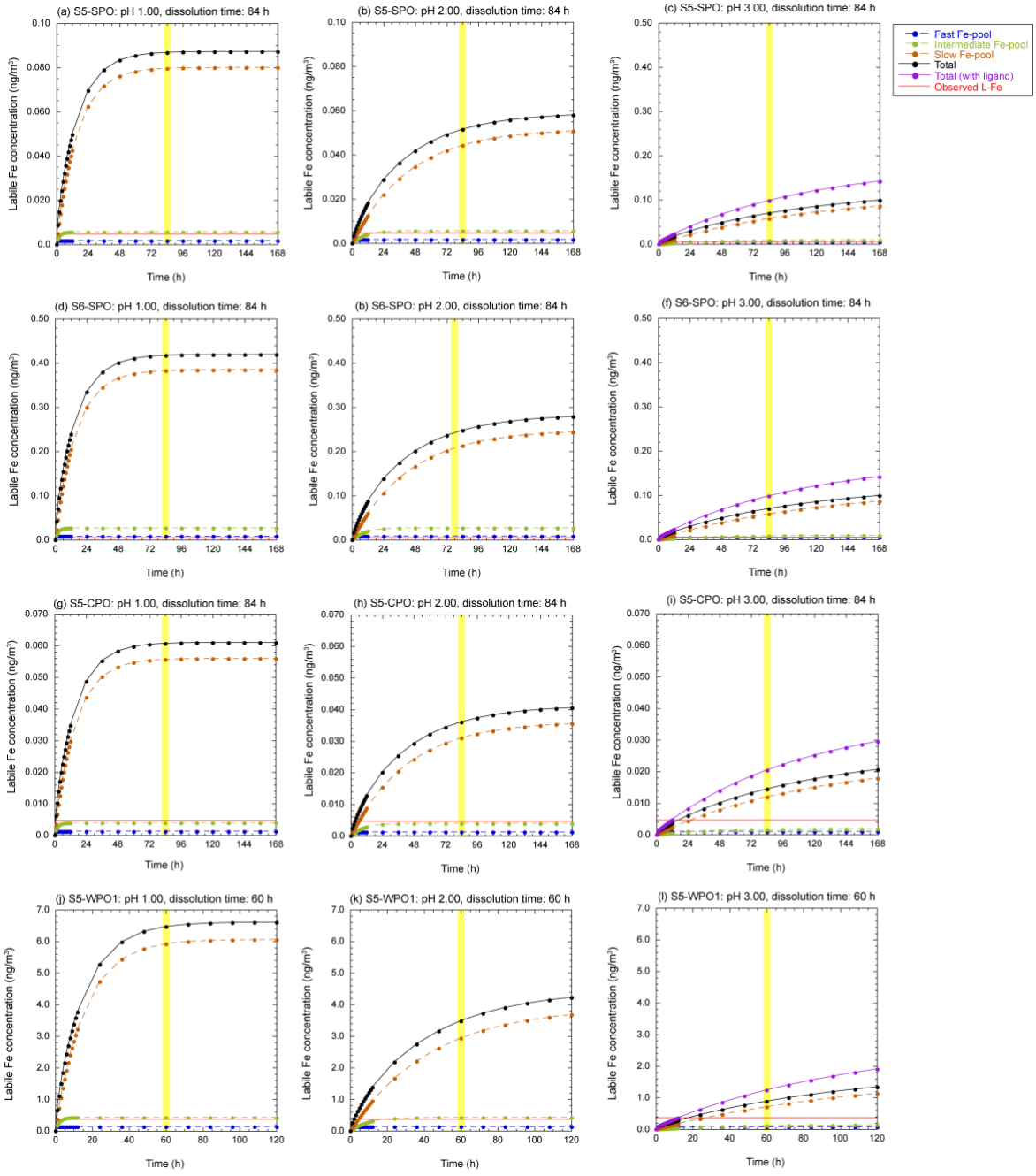

Fig. S10 Dissolution curves of L-Fe in $PM_{1.3}$ with negative $[H^+]_{mineral}$ under various pH conditions for (a-c) S5-SPO, (d-f) S6-SPO, (g-i) S5-CPO, and (j-l) S5-WPO1. The yellow shaded region in each panel shows the expected reaction time for the proton-promoted dissolution. For comparison, the total amount of Fe dissolution with consideration of ligand-promoted process at pH 3.0 is shown in the purple curve.

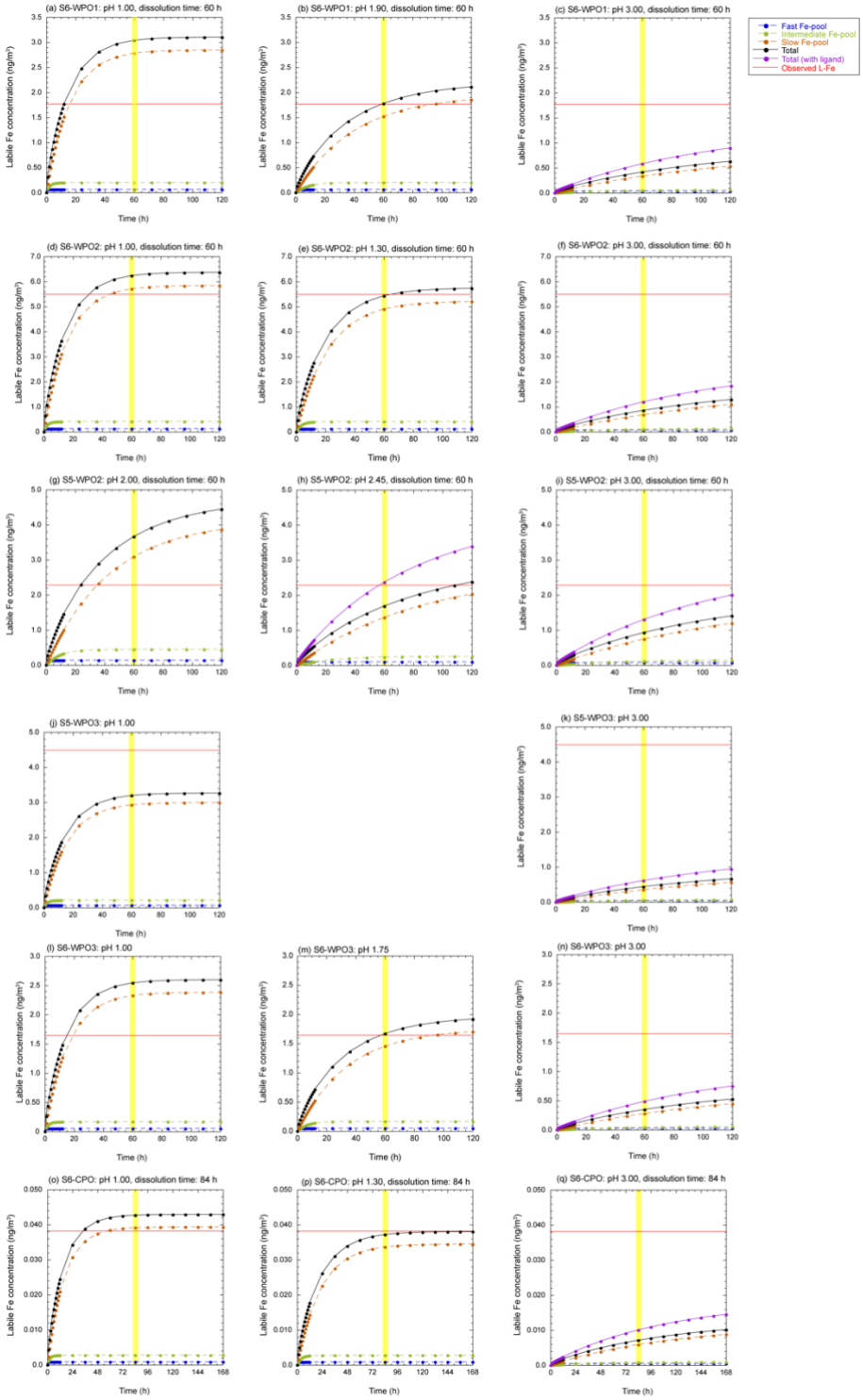

Fig. S11 Dissolution curves of L-Fe in $PM_{1.3}$ with positive $[H^+]_{mineral}$ under various pH conditions for (a-c) S6-WPO1, (d-f) S6-WPO2, (g-h) S5-WPo2, (j and k) S5-WPO3, (l-n) S6-WPO3, and (o-q) S6-CPO. The yellow shaded region in each panel shows the expected reaction time for the proton-promoted dissolution.

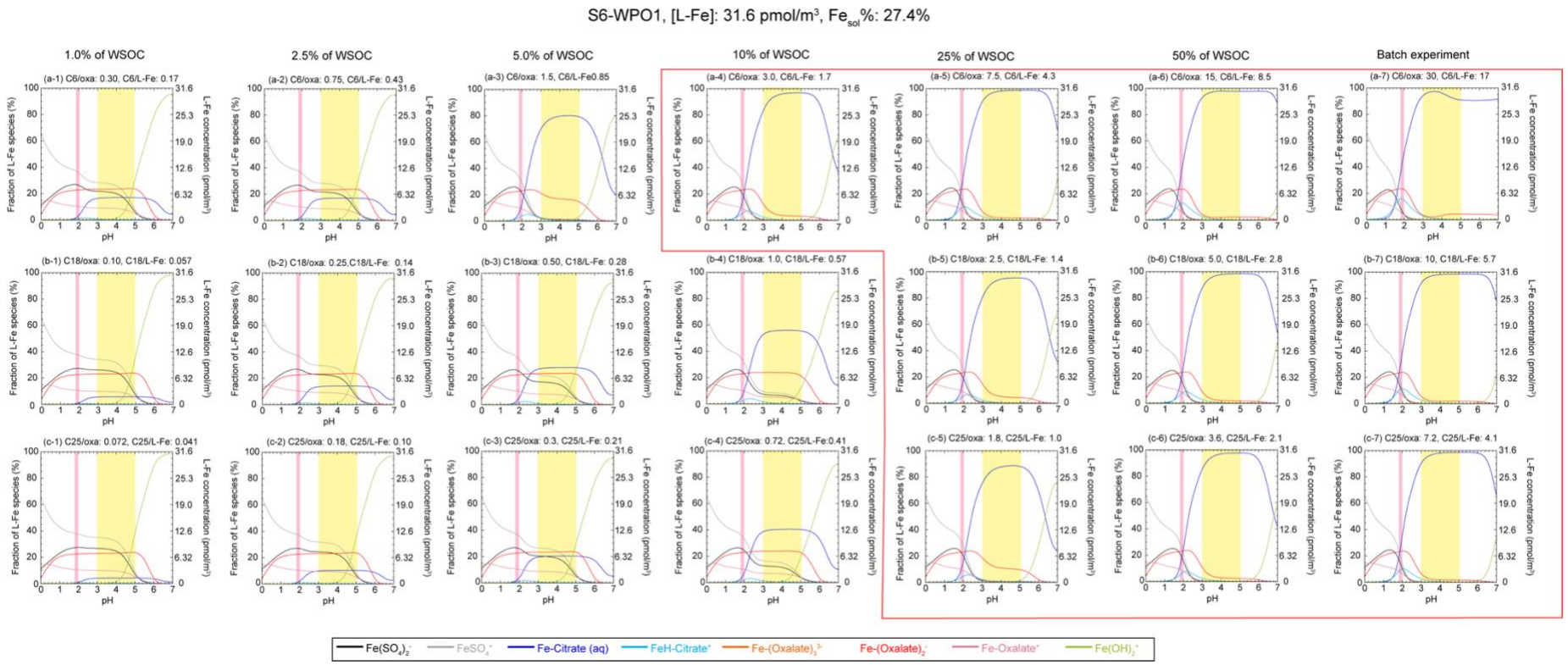

Fig. S12 pH dependences of L-Fe species in S6-WPO1 under different carbon numbers of WSOC and molar ratio of WSOC/oxalate. (a-1 to a-7) citric acid: C6, (b-1 to b-7) marine aliphatic carbon: C18, and (c-1 and c-7) deferoxamine: C25. Pink and yellow region shows aerosol pH for proton-promoted dissolutions and stable pH regions of Fe(III)-HULIS, respectively. The figures showing the agreement between the labile Fe species determined by XAFS spectroscopy (Fe(III)-HULIS) and the calculated results is surrounded by a red square.

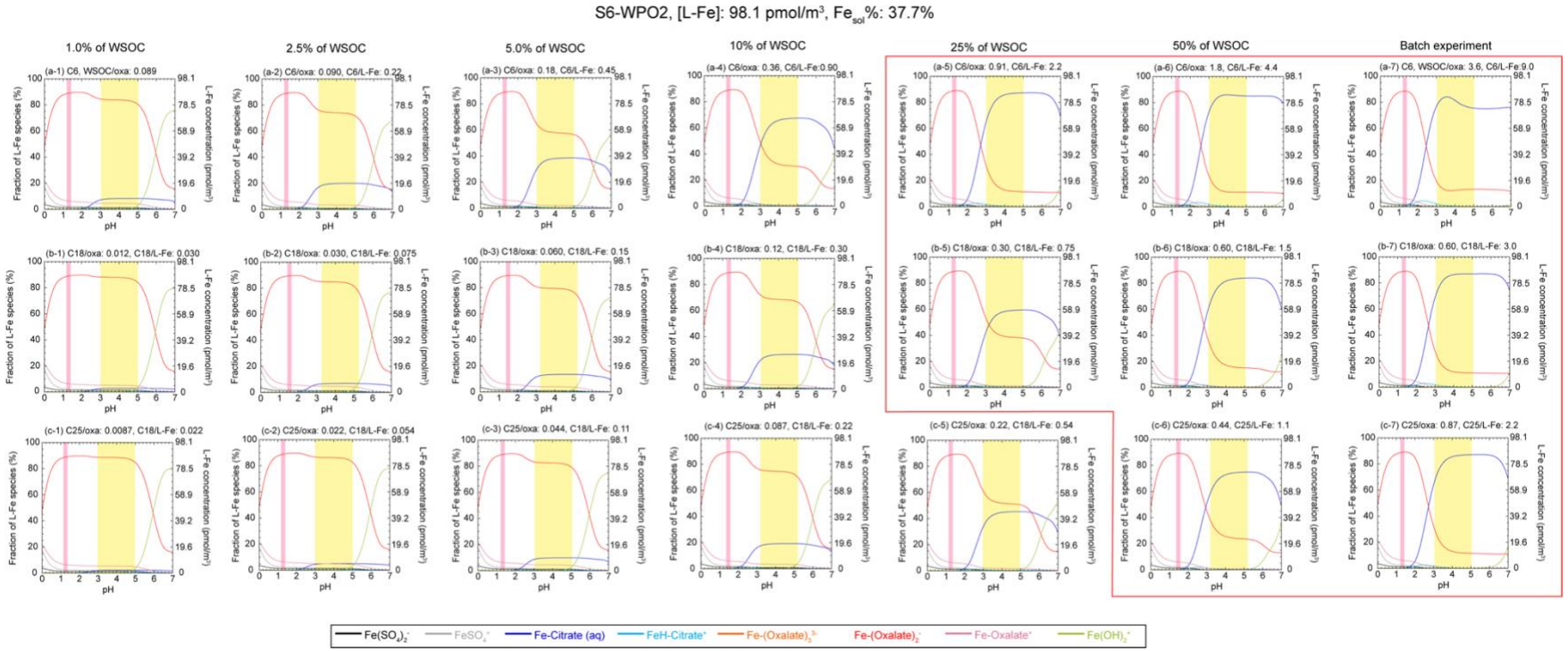

Fig. S13 pH dependences of L-Fe species in S6-WPO2 under different carbon numbers of WSOC and molar ratio of WSOC/oxalate. (a-1 to a-7) citric acid: C6, (b-1 to b-7) marine aliphatic carbon: C18, and (c-1 and c-7) deferoxamine: C25. Pink and yellow region shows aerosol pH for proton-promoted dissolutions and stable pH regions of Fe(III)-HULIS, respectively. The figures showing the agreement between the labile Fe species determined by XAFS spectroscopy (Fe(III)-HULIS) and the calculated results is surrounded by a red square.

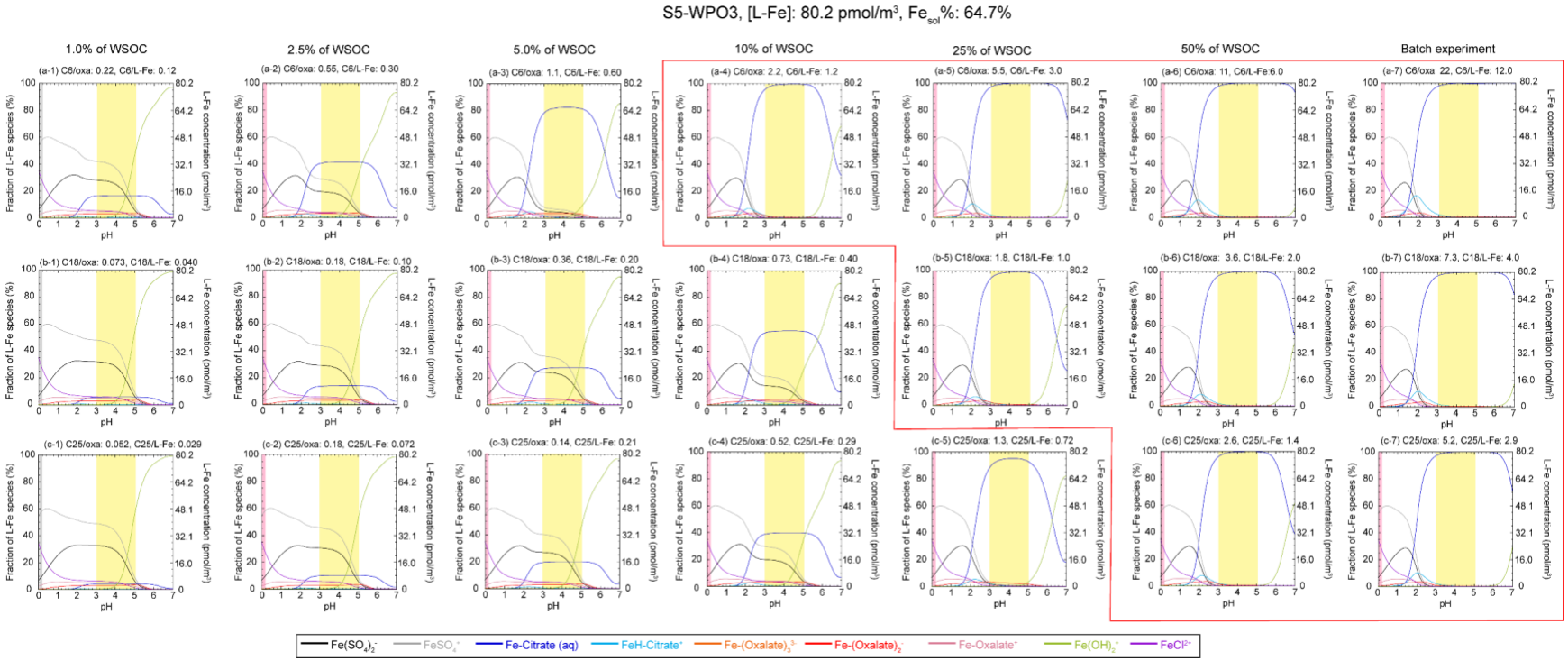

Fig. S14 pH dependences of L-Fe species in S5-WPO3 under different carbon numbers of WSOC and molar ratio of WSOC/oxalate. (a-1 to a-7) citric acid: C6, (b-1 to b-7) marine aliphatic carbon: C18, and (c-1 and c-7) deferoxamine: C25. Pink and yellow region shows aerosol pH for proton-promoted dissolutions and stable pH regions of Fe(III)-HULIS, respectively. The figures showing the agreement between the labile Fe species determined by XAFS spectroscopy (Fe(III)-HULIS) and the calculated results is surrounded by a red square.

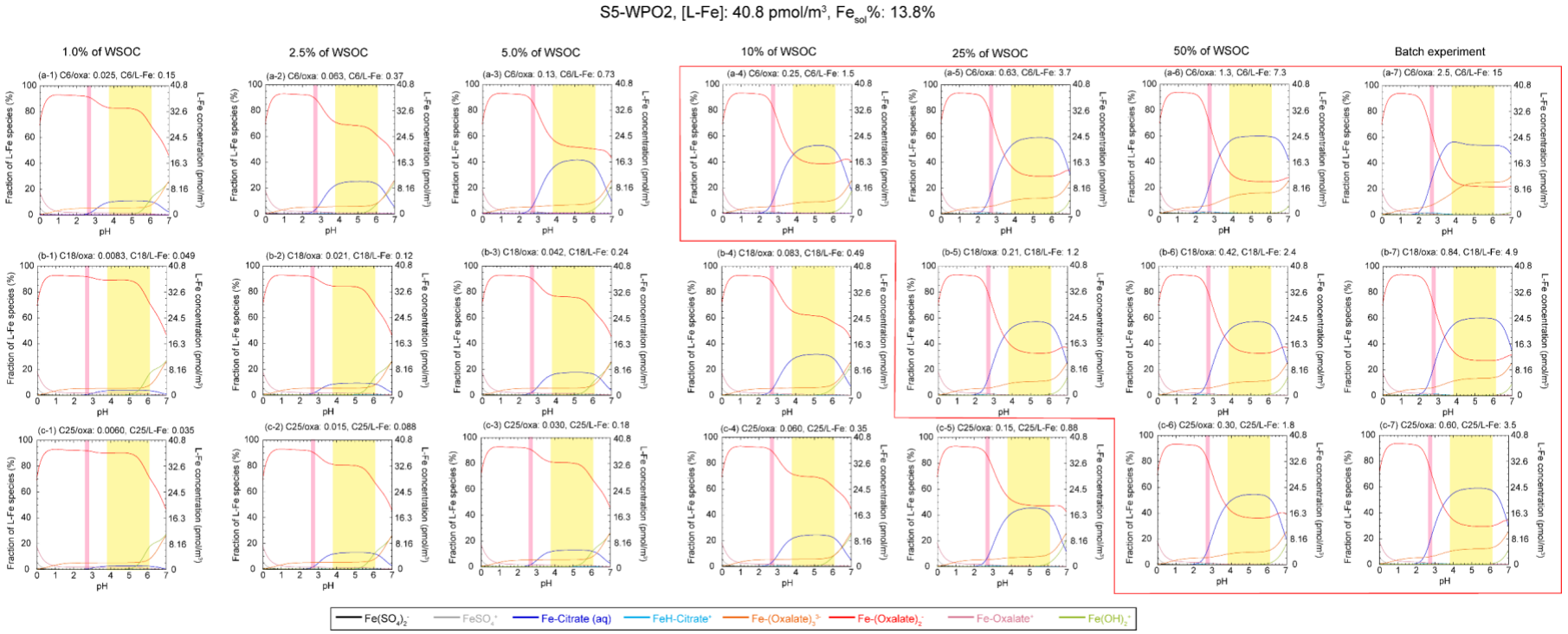

Fig. S15 pH dependences of L-Fe species in S5-WPO2 under different carbon numbers of WSOC and molar ratio of WSOC/oxalate. (a-1 to a-7) citric acid: C6, (b-1 to b-7) marine aliphatic carbon: C18, and (c-1 and c-7) deferoxamine: C25. Pink and yellow region shows aerosol pH for proton-promoted dissolutions and stable pH regions of Fe(III)-HULIS, respectively. The figures showing the agreement between the labile Fe species determined by XAFS spectroscopy (Fe(III)-HULIS) and the calculated results is surrounded by a red square.

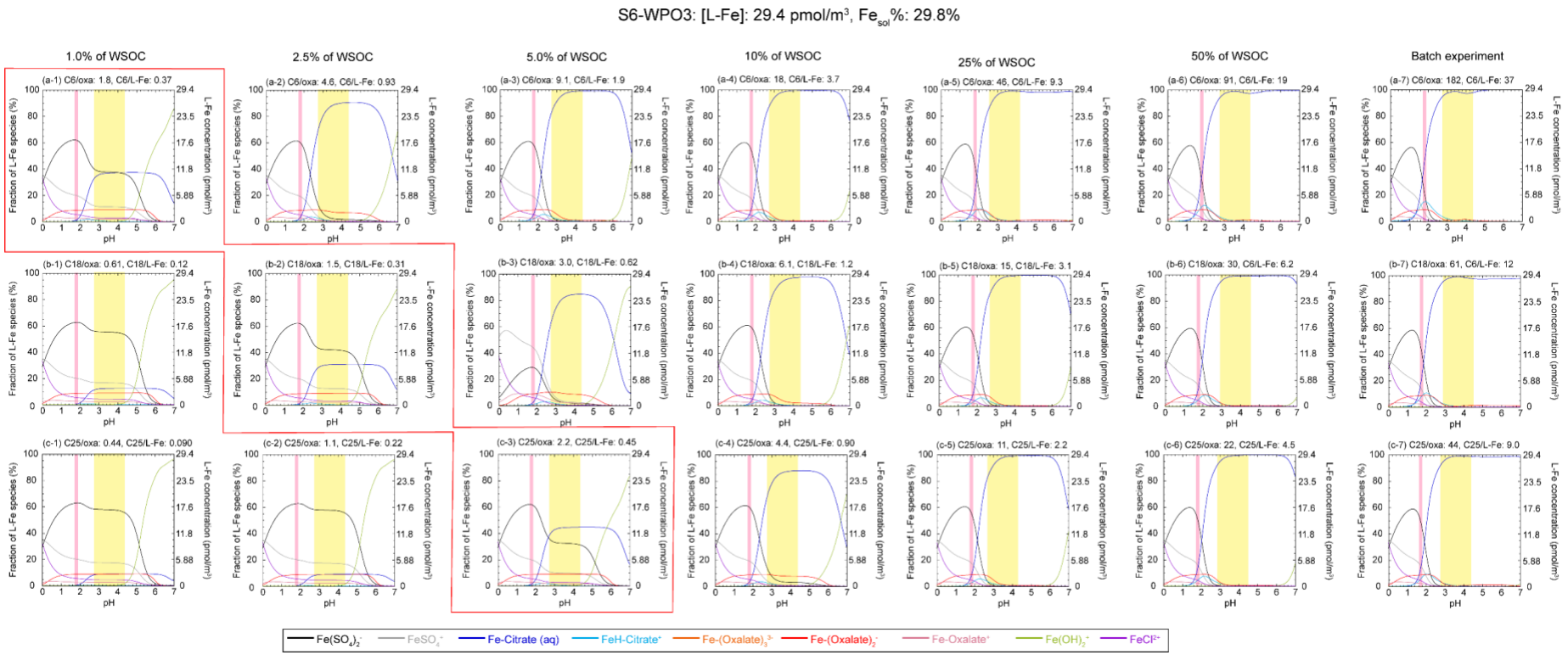

Fig. S16 pH dependences of L-Fe species in S6-WPO3 under different carbon numbers of WSOC and molar ratio of WSOC/oxalate. (a-1 to a-7) citric acid: C6, (b-1 to b-7) marine aliphatic carbon: C18, and (c-1 and c-7) deferoxamine: C25. Pink and yellow region shows aerosol pH for proton-promoted dissolutions and stable pH regions of Fe(III)-HULIS, respectively. The figures showing the agreement between the labile Fe species determined by XAFS spectroscopy (Fe(III)-HULIS and Fe(III)-sulfate) and the calculated results is surrounded by a red square.

Table S1. Aerosol diameter and filter materials for each sampling stage.

	Aerosol diameter (μm)	Filter material
Stage-1 (S1)	Larger than 10.2	PTFE
Stage-2 (S2)	4.2 to 10.2	PTFE
Stage-3 (S3)	2.1 to 4.2	PTFE
Stage-4 (S4)	1.3 to 2.1	PTFE
Stage-5 (S5)	0.69 to 1.3	PTFE
Stage-6 (S6)	0.39 to 0.69	PTFE
Stage-7 (S7)	Finer than 0.39	Cellulose

Table S2. Sampling information of the size-fractionated aerosols used in this study.

	Start			End			
	Time, Date (GMT)	Latitude	Longitude	Time, Date (GMT)	Latitude	Longitude	Total flow (m^3)
SPO	4:39, Jan. 10	49.39º S	170.00º W	11:40, Jan. 14	32.37º S	170.00º W	2256.1
CPO	20:41, Jan. 27	29.57º S	170.00º W	1:25, Feb. 1	15.07º S	170.00º W	1923.2
WPO1	5:35, Feb. 16	9.11º N	159.18º E	20:21, Feb. 18	12.42º N	143.36º E	1739.5
WPO2	19:29, Feb. 19	13.34º N	144.02º E	19:29, Feb. 21	21.25º N	144.03º E	1215.6
WPO3	9:59, Feb. 22	21.46º N	143.58º E	10:42, Feb. 24	32.07º N	140.47º E	973.0

Table S3. Correlation matrix (Spearman's rho) of Fe_{sol}%, EF of trace metals, and molar concentrations of [nss-SO_4^{2-}] and [oxalate].

	Fe_{sol}%	Ti	V	Mn	Fe	Co	Ni	Cu	Zn	Cd	Pb
Fe_{sol}%	1.00										
Ti	0.14	1.00									
V	0.36	-0.05	1.00								
Mn	-0.31	***-0.83***	-0.04	1.00							
Fe	-0.27	-0.19	***-0.76***	0.41	1.00						
Co	-0.26	0.15	0.60	0.02	-0.28	1.00					
Ni	-0.25	-0.02	0.56	0.25	-0.20	***0.92***	1.00				
Cu	0.07	0.09	0.03	-0.01	0.18	0.12	0.37	1.00			
Zn	-0.09	-0.60	0.59	***0.70***	-0.14	0.54	***0.73***	0.20	1.00		
Cd	0.62	-0.24	-0.10	0.22	0.44	-0.44	-0.30	0.33	0.01	1.00	
Pb	***0.75***	-0.14	0.12	-0.12	0.07	-0.47	-0.43	0.27	-0.16	***0.84***	1.00
[nss-SO_4^{2-}]	***0.81***	-0.10	0.04	-0.13	0.15	-0.48	-0.49	0.09	-0.21	***0.87***	***0.95***
[Oxalate]	0.20	0.02	**-0.70**	-0.29	0.30	-0.86	***-0.90***	-0.16	***-0.75***	0.26	0.37

Correlation coefficients with p-values smaller than 0.05 are shown in bold and italic.

Appendix: Stability constants (log K) of main species in this study (only show 25ºC).

	Species	Reaction	Log K
		Fe species	
1.	$FeOH^+$	$Fe^{2+} + H_2O \rightarrow FeOH^+$	9.40
2.	$FeOH^{2+}$	$Fe^{3+} + H_2O \rightarrow FeOH^{2+}$	2.02
3.	$Fe(OH)_2$ (aq)	$Fe^{2+} + 2H_2O \rightarrow Fe(OH)_2$ (aq) $+ 2H^+$	20.5
4.	$Fe(OH)_2^+$	$Fe^{3+} + 2H_2O \rightarrow Fe(OH)_2^+ + 2H^+$	5.75
5.	$Fe(OH)_3^-$	$Fe^{2+} + 3H_2O \rightarrow Fe(OH)_3^-$ (aq) $+ 3H^+$	31.0
6.	$Fe(OH)_3$ (aq)	$Fe^{3+} + 3H_2O \rightarrow Fe(OH)_3^+ + 3H^+$	15.0
7.	$Fe(OH)_4^-$	$Fe^{3+} + 4H_2O \rightarrow Fe(OH)_4^- + 4H^+$	22.7
9.	$Fe_2(OH)_2^{4+}$	$2Fe^{3+} + 2H^+ + 2H_2O \rightarrow Fe_2(OH)_2^{4+}$	2.89
9.	Fe-$(oxalate)_2^-$	$Fe^{3+} + 2\cdot Oxalate^{2-} \rightarrow$ Fe-$(oxalate)_2^-$	15.5
10.	Fe-$(oxalate)_2^{2-}$	$Fe^{2+} + 2\cdot Oxalate^{2-} \rightarrow$ Fe-$(oxalate)_2^{2-}$	5.90
11.	Fe-$(oxalate)_3^{3-}$	$Fe^{3+} + 3\cdot Oxalate^{2-} \rightarrow$ Fe-$(oxalate)_3^{3-}$	19.8
12.	Fe-oxalate (aq)	$Fe^{2+} + Oxalate^{2-} \rightarrow$ Fe-oxalate (aq)	3.97
13.	Fe-$oxalate^+$	$Fe^{3+} + Oxalate^{2-} \rightarrow$ Fe-$oxalate^+$	9.15
14.	Fe-$citrate^-$	$Fe^{2+} + Citrate^{3-} \rightarrow$ Fe-$citrate^-$	5.89
15.	Fe-citrate (aq)	$Fe^{3+} + Citrate^{3-} \rightarrow$ Fe-citrate (aq)	13.1
16.	FeH-citrate (aq)	$Fe^{2+} + H^+ + Citrate^{3-} \rightarrow$ FeH-citrate (aq)	10.2
17.	FeH-$citrate^+$	$Fe^{3+} + H^+ + Citrate^{3-} \rightarrow$ FeH-$citrate^+$	10.2
18.	Fe(OH)-$citrate^-$	$Fe^{3+} + Citrate^{3-} + H_2O \rightarrow$ Fe(OH)-$citrate^-$	1.79
19.	$FeSO_4$ (aq)	$Fe^{2+} + SO_4^{2-} \rightarrow FeSO_4$ (aq)	2.39
20.	$FeSO_4^+$	$Fe^{3+} + SO_4^{2-} \rightarrow FeSO_4^+$	4.25
21.	$Fe(SO_4)_2^-$	$Fe^{3+} + 2SO_4^{2-} \rightarrow Fe(SO_4)_2^-$	5.38
22.	$FeCl^+$	$Fe^{2+} + Cl^- \rightarrow FeCl^+$	0.200
23.	$FeCl^{2+}$	$Fe^{3+} + Cl^- \rightarrow FeCl^{2+}$	1.48
		Al species	
24.	$AlOH^{2+}$	$Al^{3+} + H_2O \rightarrow AlOH^{2+} + H^+$	5.00
25.	$Al(OH)_2^+$	$Al^{3+} + 2H_2O \rightarrow Al(OH)_2^+ + 2H^+$	10.3
26.	$Al(OH)_3$ (aq)	$Al^{3+} + 3H_2O \rightarrow Al(OH)_3$ (aq) $+ 3H^+$	16.7

Appendix: Continued.

	Species	Reaction	Log K
27.	$Al(OH)_4^-$	$Al^{3+} + 4H_2O \rightarrow Al(OH)_4^- 4H^+$	23.0
28.	$AlSO_4^+$	$Al^{3+} + SO_4^{2-} \rightarrow AlSO_4^+$	3.81
29.	$Al(SO_4)_2^-$	$Al^{3+} + 2SO_4^{2-} \rightarrow Al(SO_4)_2^-$	5.58
30.	Al-oxalate$^+$	$Al^{3+} + Oxalate^{2-} \rightarrow$ Al-oxalate$^-$	7.73
31.	Al-$(oxalate)_2^-$	$Al^{3+} + 2{\cdot}Oxalate^{2-} \rightarrow$ Al-$(oxalate)_2^-$	13.4
32.	Al-$(oxalate)_3^-$	$Al^{3+} + 3{\cdot}Oxalate^{2-} \rightarrow$ Al-$(oxalate)_3^{3-}$	17.1
33.	AlOH-oxalate (aq)	$Al^{3+} + Oxalate^{2-} + H_2O \rightarrow$ AlOH-oxalate (aq)	2.57
34.	Al-citrate (aq)	$Al^{3+} + Citrate^{3-} \rightarrow$ Al-citrate (aq)	9.98
35.	Al-$(citrate)_2^{3-}$	$Al^{3+} + 2{\cdot}Citrate^{3-} \rightarrow$ Al-$(citrate)_2^{3-}$ (aq)	14.8
36.	AlH-citrate$^+$	$Al^{3+} + Citrate^{3-} + H^+ \rightarrow$ AlH-citrate$^+$	12.9
37.	$AlCl^{2+}$	$Al^{3+} + Cl^- \rightarrow AlCl^{2+}$	0.390
		Cu species	
38.	$CuOH^+$	$Cu^{2+} + H_2O \rightarrow CuOH^+ + H^+$	7.45
39.	$Cu(OH)_2$ (aq)	$Cu^{2+} + 2H_2O \rightarrow Cu(OH)_2$ (aq) $+ H^+$	16.23
40.	$Cu(OH)_3^-$	$Cu^{2+} + 3H_2O \rightarrow Cu(OH)_3^- + 2H^+$	26.6
41.	$Cu(OH)_4^{2-}$	$Cu^{2+} + 4H_2O \rightarrow Cu(OH)_4^{2-} + 3H^+$	39.7
42.	$CuSO_4$ (aq)	$Cu^{2+} + SO^{2-} \rightarrow CuSO_4$ (aq)	2.36
43.	Cu-oxalate (aq)	$Cu^{2+} + oxalate^{2-} \rightarrow$ Cu-oxalate (aq)	5.72
44.	Cu-$(oxalate)_2^{2-}$	$Cu^{2+} + 2{\cdot}oxalate^{2-} \rightarrow$ Cu-$(oxalate)_2^{2-}$	10.2
45.	Cu-citrate$^-$	$Cu^{2+} + citrate^{3-} \rightarrow$ Cu-citrate$^-$	7.57
46.	Cu-$(citrate)_2^{3-}$	$Cu^{2+} + 2{\cdot}citrate^{3-} \rightarrow$ Cu-$(citrate^-)_2^{3-}$	8.90
47.	Cu_2-$(citrate)_2^{2-}$	$2Cu^{2+} + 2{\cdot}citrate^{3-} \rightarrow Cu_2$-$(citrate)_2^{2-}$	16.9
48.	CuCl (aq)	$Cu^+ + Cl^- \rightarrow$ CuCl (aq)	3.10
49.	$CuCl^+$	$Cu^{2+} + Cl^- \rightarrow CuCl^+$	0.300
50.	$CuCl_2^-$	$Cu^+ + 2Cl^- \rightarrow CuCl_2^-$	5.42
51.	$CuCl_2$ (aq)	$Cu^{2+} + 2Cl^- \rightarrow CuCl_2$ (aq)	0.260
52.	$CuCl_3^{2-}$	$Cu^+ + 3Cl^- \rightarrow CuCl_3^{2-}$	2.29
53.	$CuCl_3^-$	$Cu^{2+} + 3Cl^- \rightarrow CuCl_3^-$	4.75
54.	$CuCl_4^{2-}$	$Cu^{2+} + 4Cl^- \rightarrow CuCl_4^{2-}$	-4.59

Appendix: Continued.

	Species	Reaction	Log K
55.	$CuNH_3^{2+}$	$Cu^{2+} + NH_4^+ \rightarrow CuNH_3^{2+} + H^+$	5.22
56.	$Cu(NH_3)_2^+$	$Cu^+ + 2NH_4^+ \rightarrow Cu(NH_3)_2^+ + 2H^+$	0.680
57.	$Cu(NH_3)_2^{2+}$	$Cu^{2+} + 2NH_4^+ \rightarrow Cu(NH_3)^{2+} + 2H^+$	11.1
58.	$Cu(NH_3)_3^{2+}$	$Cu^{2+} + 3NH_4^+ \rightarrow Cu(NH_3)^{2+} + 3H^+$	17.5
59.	$Cu(NH_3)_4^{2+}$	$Cu^{2+} + 4NH_4^+ \rightarrow Cu(NH_4)^{2+} + 4H^+$	24.7
		H species	
60.	H-oxalate$^-$	$H^+ + oxalate^{2-} \rightarrow$ H-oxalate$^-$	4.27
61.	H_2-oxalate (aq)	$2H^+ + oxalate^{2-} \rightarrow H_2$-oxalate (aq)	5.52
62.	H-citrate^{2-}	$H^+ + citrate^{3-} \rightarrow$ H-citrate^{2-}	6.40
63.	H_2-citrate$^-$	$2H^+ + citrate^{3-} \rightarrow H_2$-citrate$^-$	11.2
64.	H_3-citrate (aq)	$3H^+ + citrate^{3-} \rightarrow H_3$-citrate (aq)	14.3
		Other species	
65.	$NH_4SO_4^-$	$NH_4^+ + SO_4^{2-} \rightarrow NH_4SO_4^-$	1.03
66.	NH_4-oxalate$^-$	$NH_4^+ + oxalate^{2-} \rightarrow NH_4$-oxalate$^-$	0.900
67.	NaCl(aq)	$Na^+ + Cl^- \rightarrow$ NaCl (aq)	0.300
68.	$NaNO_3$ (aq)	$Na^+ + NO_3^- \rightarrow NaNO_3$ (aq)	0.550
69.	$NaSO_4^-$	$Na^+ + SO_4^{2-} \rightarrow NaSO_4^-$	0.740
70.	Na-oxalate$^-$	$Na^+ + oxalate^{2-} \rightarrow$ Na-oxalate$^-$	0.900
71.	Na-citrate^{2-}	$Na^+ + citrate^{3-} \rightarrow$ Na-citrate^{2-}	1.39
72.	KCl (aq)	$K^+ + Cl^- \rightarrow$ KCl (aq)	-0.300
73.	KNO_3 (aq)	$K^+ + NO_3^- \rightarrow KNO_3$ (aq)	-0.190
74.	KSO_4^-	$K^+ + SO_4^{2-} \rightarrow KSO_4^-$	0.847
75.	K-oxalate$^-$	$K^+ + oxalate^{2-} \rightarrow$ K-oxalate$^-$	0.800
76.	K-citrate^{2-}	$K^+ + citrate^{2-} \rightarrow$ K-citrate^{2-}	1.10
77.	$MgCl^+$	$Mg^{2+} + Cl^- \rightarrow MgCl^+$	0.600
78.	$MgSO_4$ (aq)	$Mg^{2+} + SO_4^{2-} \rightarrow MgSO_4$ (aq)	2.26
79.	Mg-oxalate (aq)	$Mg^{2+} + oxalate^{2-} \rightarrow$ Mg-oxalate (aq)	3.62
80.	Mg-citrate$^-$	$Mg^{2+} + citrate^{3-} \rightarrow$ Mg-citrate$^-$	4.89
81.	MgH-citrate (aq)	$Mg^{2+} + citrate^{3-} + H^+ \rightarrow$ MgH-citrate (aq)	8.91

Table S5. Continued.

	Species	Reaction	Log K
82.	MgH_2-citrate$^+$	$Mg^{2+} + citrate^{3-} + 2H^+ \rightarrow MgH_2$-citrate$^+$	12.3
83.	$CaCl^+$	$Ca^{2+} + Cl^- \rightarrow CaCl^+$	0.400
83.	$CaCl^+$	$Ca^{2+} + Cl^- \rightarrow CaCl^+$	0.400
84.	$CaNO_3^+$	$Ca^{2+} + NO_3^- \rightarrow CaNO_3^+$	0.500
85.	$CaSO_4$ (aq)	$Ca^{2+} + SO_4^{2-} \rightarrow CaSO_4$ (aq)	2.36
86.	Ca-oxalate (aq)	$Ca^{2+} + oxalate^{2-} \rightarrow$ Ca-oxalate (aq)	3.19
87.	Ca-citrate$^-$	$Ca^{2+} + citrate^{3-} \rightarrow$ Ca-citrate$^-$	4.87
88.	CaH-citrate (aq)	$Ca^{2+} + citrate^{3-} + H^+ \rightarrow$ CaH-citrate (aq)	9.26
89.	CaH_2-citrate$^+$	$Ca^{2+} + citrate^{3-} + 2H^+ \rightarrow CaH_2$-citrate$^+$	12.6